Design and Performance of the DSS-14 Antenna Controller

W. Gawronski,[1] H. G. Ahlstrom, Jr.,[1] and A. B. Bernardo[1]

The linear quadratic Gaussian (LQG) controller for the DSS-14 antenna was designed, and its performance was compared with the existing controller. The controller design included the antenna field testing, system identification to obtain the controller model, and the gain determination. The performance of the new controller is significantly improved over the existing one, both in the tracking and in the wind disturbance rejection properties. The performance can be improved further if the command preprocessor is installed. The preprocessor prevents limit cycling that is caused by the acceleration limits during slewing. The new controller is designed for the "computer" (or encoder-based) mode. The "precision" mode (that includes the master equatorial) needs to be investigated separately.

I. Introduction

The purpose of this investigation is to design a new controller for the DSS-14 antenna that improves the antenna tracking performance in terms of the time of response, bandwidth, and disturbance-rejection properties. This article presents the open-loop test results, the determination of the antenna-rate-loop models (in azimuth and elevation) from the test data, the linear quadratic Gaussian (LQG) controller design, and nonlinear simulations to assess the closed-loop system performance.

Experience to date with the servo performance of the beam-waveguide (BWG) antennas indicates that the LQG controller has the expected properties, such as wide bandwidth, short response time, and improved wind-disturbance rejection properties. The LQG controller is a model-based controller; that is, the plant model (or, in our case, the rate-loop model) is a part of the controller. Therefore, the rate-loop model must exactly imitate the actual antenna dynamics in order to stabilize the antenna and to achieve the best allowable performance. Analytical models (such as those developed in [1]) will not serve the purpose, since the discrepancies between the model-simulated dynamics and the actual antenna dynamics could cause a deteriorated performance and even closed-loop instability. The accurate model acceptable for the LQG controller design is obtained from antenna testing. In these tests, the responses of the antenna encoders to the white-noise-rate inputs are recorded. Using these input–output data, the analytical model is determined using a system identification procedure. Based on the obtained antenna model, the LQG controller is designed. It should have an improved performance (in properties such as bandwidth and disturbance-induced errors) and allow for slewing with the imposed rate and acceleration limits.

[1] Communications Ground Systems Section.

II. Rate-Loop Tests

The tests consisted of the injection of a white-noise signal at the antenna rate input, either in azimuth or elevation, or of the recording of the antenna encoder response, in azimuth or elevation, correspondingly. The sampling rate was 20 Hz, and the record length was over 16,000 samples. A record of such length is required to obtain comparatively smooth averages of the system transfer function and to obtain a reliable model from the system identification procedure. The input and output records of the azimuth axis testing are shown in Fig. 1.

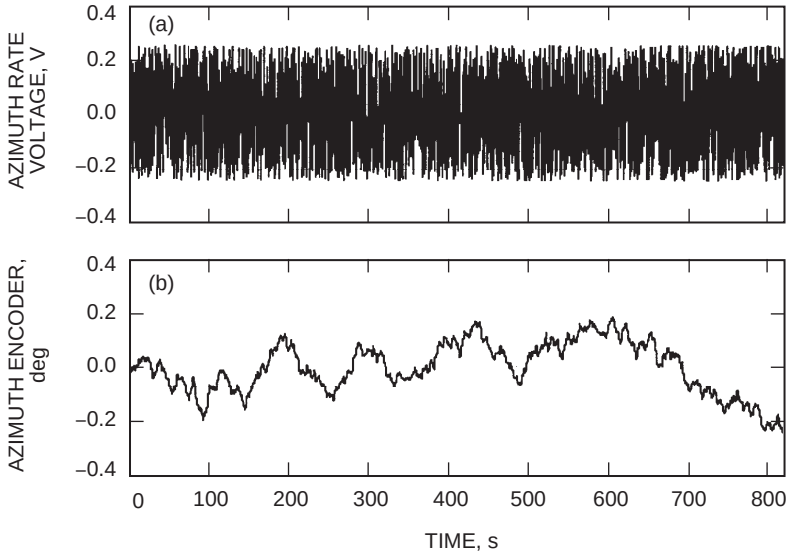

Fig. 1. The azimuth axis testing records: (a) the white noise at the rate input to the azimuth drive and (b) the azimuth encoder output.

The input data, $u(t)$, and the output data, $y(t)$, were used to determine the system transfer function. The records $u(t)$ and $y(t)$ were divided into n segments: $u_i(t)$ and $y_i(t), i = 1, \cdots, n$, of length T. Next, we obtained a "smooth" estimate of the input and output cross-spectral density function,

$$P_{uy}(\omega) = \frac{2}{nT} \sum_{i=1}^{n} u_i^*(\omega) y_i(\omega) \tag{1}$$

along with the estimate of the input autospectral density function,

$$P_u(\omega) = \frac{2}{nT} \sum_{i=1}^{n} |u_i(\omega)|^2 \tag{2}$$

where $u_i(\omega)$ and $y_i(\omega)$ are Fourier transforms of $u_i(t)$ and $y_i(t)$, respectively, and u^* denotes the complex conjugate transpose of u. The estimate $\overline{G}(\omega)$ of the transfer function $G(\omega)$ is obtained as follows:

$$\overline{G}(\omega) = \frac{P_{uy}(\omega)}{P_u(\omega)} \tag{3}$$

The above procedure can be executed with the Matlab subroutine *spectrum*:

$$P = \ spectrum\ (u, y, N) \tag{4}$$

where N is the length of the segment (we used $N = 2^{10} = 1024$). The output matrix P consists of 8 columns: the first column is $P_u(\omega)$, the second is $P_{uy}(\omega)$, the third is $\overline{G}(\omega)$, and the fourth is the coherence between u and y.

The quality of the data is determined by their coherence function versus frequency. The value of the coherence function is 1 if the input and output are linearly dependent and no disturbances are recorded. It is much less than 1 if the input and output are nonlinearly coupled and/or there are disturbances in the data. Figure 2 shows the magnitude and phase of the transfer function, $\overline{G}(\omega)$, and Fig. 3 shows the coherence function for the records as in Fig. 1. The coherence is greater than 0.9 for the frequency range up to 2 Hz (except for the segments where the magnitude of $\overline{G}(\omega)$ drops significantly).

Similar results were obtained for the elevation-axis tests. The plots of the magnitude and phase of the elevation computer transfer function are shown in Fig. 4.

The records of the encoder outputs are used in the identification of the computer mode of the antenna, wherein the encoders are used to measure the antenna position. In order to identify the precision mode

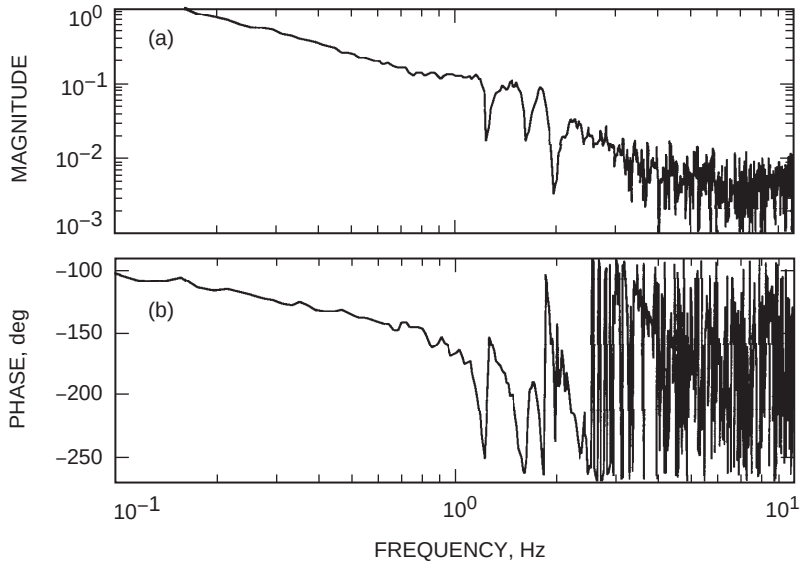

Fig. 2. The azimuth rate-loop transfer function obtained from the test data: (a) magnitude and (b) phase.

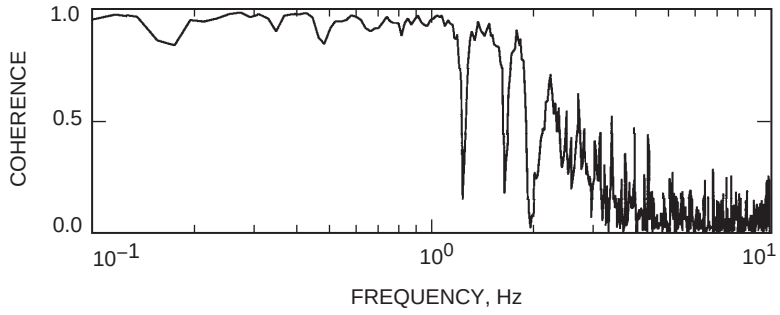

Fig. 3. The coherence function for the azimuth input and output.

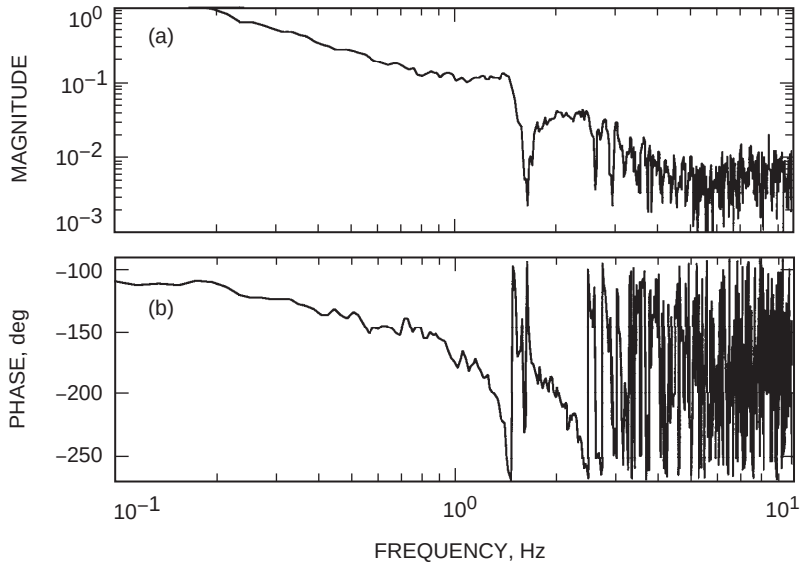

Fig. 4. The elevation rate-loop transfer function obtained from the test data: (a) magnitude and (b) phase.

of the antenna, the master equatorial (ME) responses to the white noise need to be recorded. So far, we have not succeeded in obtaining a coherent set of ME data. The antenna drift during the test was blamed for the low coherence of the ME position and the rate-input noise.

III. System Identification

The recorded data are used to determine the analytical model of the antenna in the form of its state–space representation. The ERA identification algorithm, described in [2], was used to process the data and to determine the model. The Matlab code SOCIT that uses the ERA algorithm was used to obtain the state–space representation. Then, the dimension of the state–space representation was reduced, using the balanced-state representation, as described in [3]. The resulting state–space representation is of dimension 6, both in azimuth and elevation. The magnitudes of the transfer functions of the identified models in azimuth and elevation are shown in Figs. 5 and 6, respectively. They are compared with the measured transfer functions, showing satisfactory coincidence.

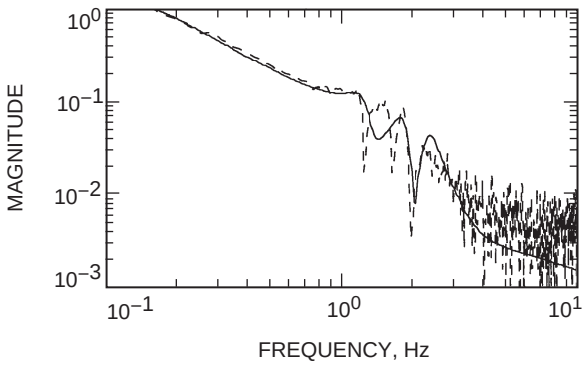

Fig. 5. Magnitudes of the azimuth-axis transfer functions from the input–output data (dashed line) and the identified model (solid line).

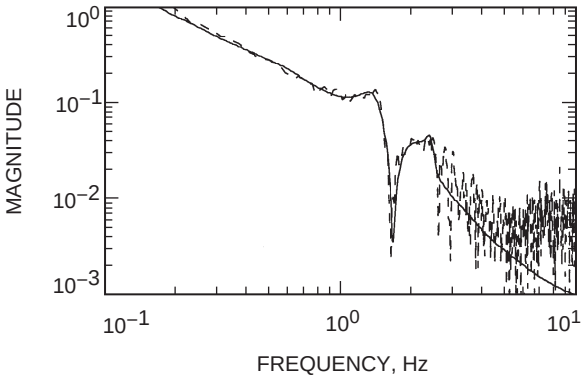

Fig. 6. Magnitudes of the elevation-axis transfer functions from the input–output data (dashed line) and the identified model (solid line).

IV. LQG Controllers—A Performance Comparison

The LQG controllers for the azimuth and elevation axes are designed based on the identified rate-loop models. The block diagram of the LQG controller is shown in Fig. 7. It consists of a proportional-and-integral (PI) controller, a flexible-mode controller, and the state estimator. The gains of the controller are determined by choosing proper weights of the controller index, as described in [4]. The step responses of the LQG controller are shown in Fig. 8 for the azimuth axis and in Fig. 9 for the elevation axis. From these plots, it follows that the overshoot is 20 percent, and the settling time is 6 s in both axes. The magnitudes of the closed-loop transfer function from the command to the encoder are shown in Figs. 10 (azimuth axis) and 11 (elevation axis). From these figures, it follows that the antenna bandwidth is 0.35 Hz.

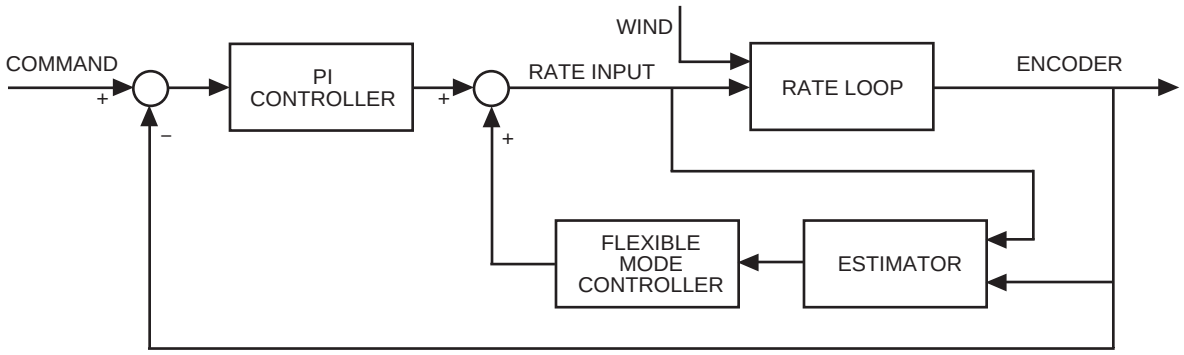

Fig. 7. The LQG controller structure.

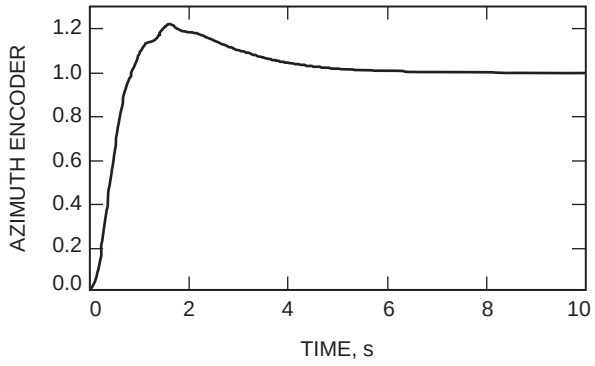

Fig. 8. Step response of the azimuth controller.

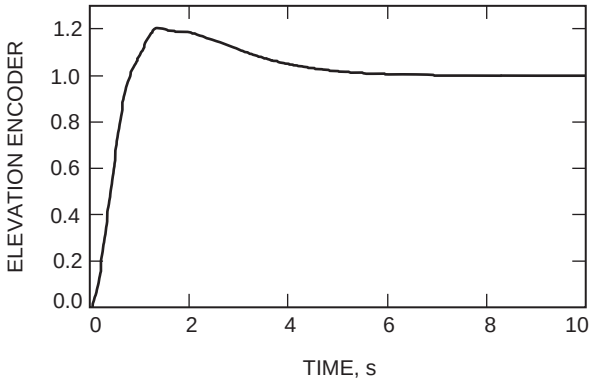

Fig. 9. Step response of the elevation controller.

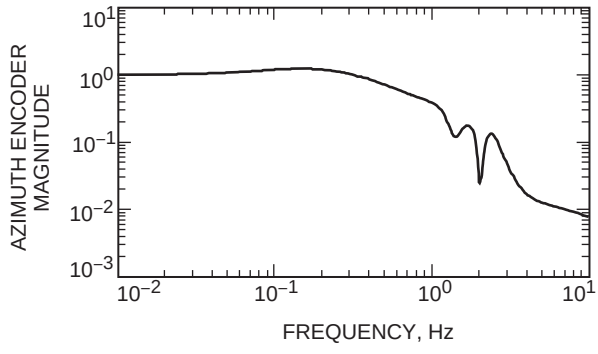

Fig. 10. Magnitude of the closed-loop transfer function, azimuth axis.

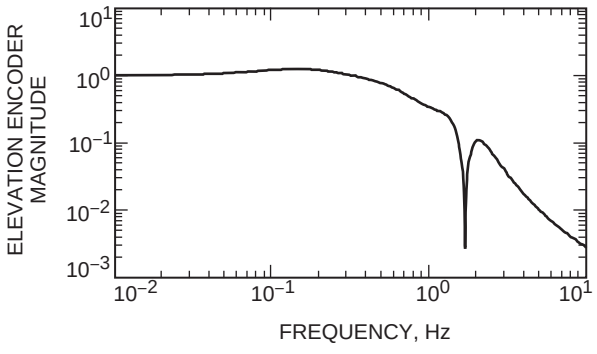

Fig. 11. Magnitude of the closed-loop transfer function, elevation axis.

The performance of the proposed design is compared with the existing controller. The step responses of the proposed design (solid line) and the existing controller (dashed line) are shown in Figs. 12 (azimuth axis) and 13 (elevation axis). The figures show that the overshoot of the proposed controller is reduced slightly (from 25 to 20 percent), and the settling time is more significantly reduced (from 10 to 6 s).

The closed-loop response to the rate offset of 10 mdeg/s of the proposed design (solid line) and the existing controller (dashed line) are shown in Figs. 14 (azimuth axis) and 15 (elevation axis). The figures show that the peak error of the proposed controller is reduced by 40 percent, and the settling time also is reduced by 40 percent, from 10 to 6 s. For larger (100-mdeg/s) rate offsets, the errors are shown in Fig. 16. The existing controller shows a steady-state error over 50 mdeg, while the proposed one has zero steady-state error. The nonzero error of the existing controller is caused by the imposed limit of 0.1 mdeg $\times$ s on the integral of the error. This limit has an impact on the performance of the existing controller and no impact on the performance of the proposed controller.

The performances of the controllers are compared for the large step offsets of 1 deg, which are used predominantly for slewing of the antenna. The results are shown in Fig. 17. The proposed controller shows limit cycling at the end of the slewing. This limit cycling is caused by the imposed acceleration limit of 0.2 deg/s^2. This can be corrected in two ways—either by raising the acceleration limit to 0.3 deg/s^2 or by implementing the command preprocessor so that the command does not exceed the limit.

The important issue is the ability of a controller to suppress the disturbances. The main disturbance of the DSS-14 antenna is wind. The wind pressure acts at the surface of the antenna structure. It is

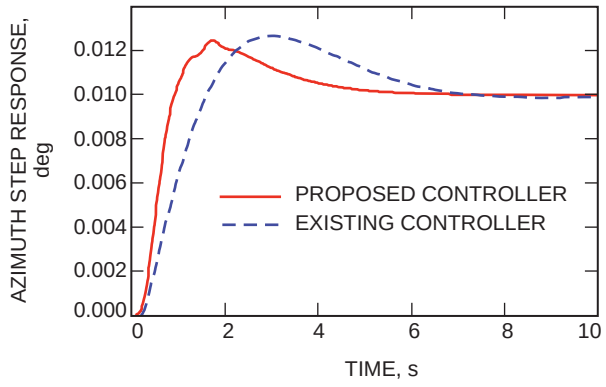

Fig. 12. Step responses of the proposed and existing azimuth controllers.

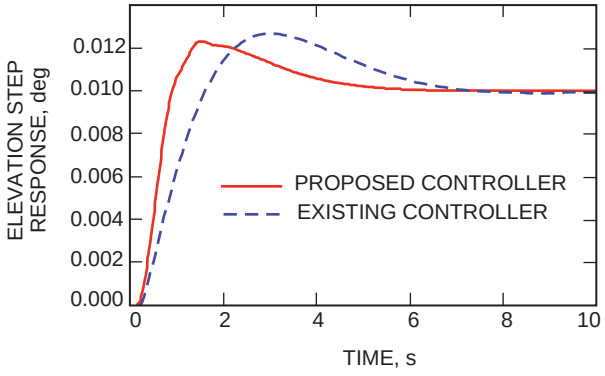

Fig. 13. Step responses of the proposed and existing elevation controllers.

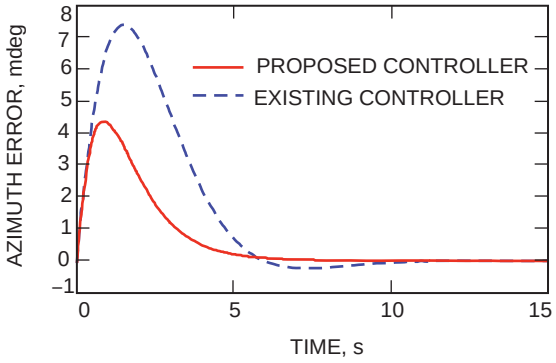

Fig. 14. Encoder errors for the 10-mdeg/s rate offset of the proposed and existing azimuth controllers.

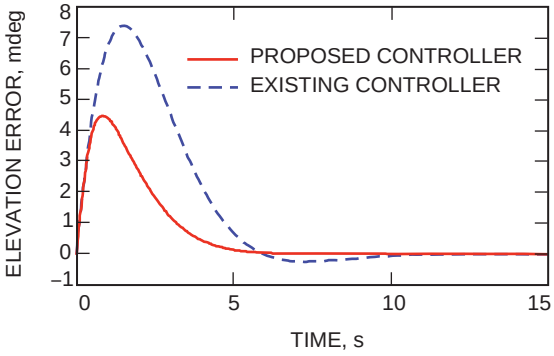

Fig. 15. Encoder errors for the 10-mdeg/s rate offset of the proposed and existing elevation controllers.

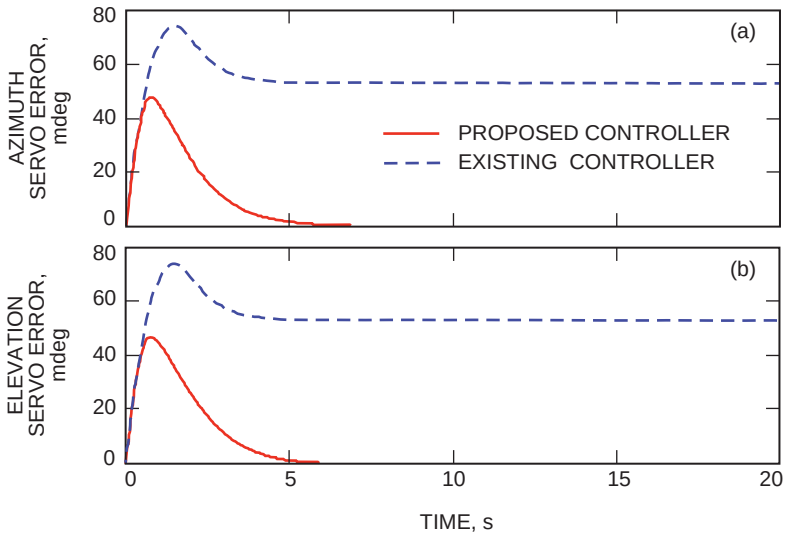

Fig. 16. Encoder errors for the 100-mdeg/s rate offset of the proposed and existing (a) azimuth and (b) elevation controllers.

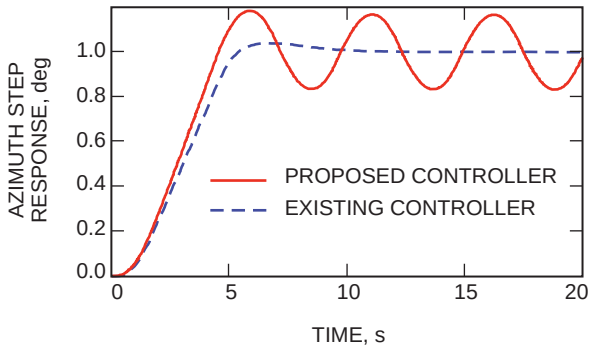

Fig. 17. The 1-deg step responses of the proposed and existing azimuth controller.

customary to model wind disturbance as a rate input to the antenna model (see [5]). The wind action can be separated as a semisteady disturbance, which we model as a step disturbance, and as a higher-frequency gust, which we model as a white-noise disturbance.

The response of the antenna azimuth encoder to the step disturbance in azimuth is shown in Fig. 18, with the solid line representing the new controller and the broken line the existing controller. The response of the antenna elevation encoder to the step disturbance in the elevation direction is shown in Fig. 19, with the solid line representing the new controller and the broken line the existing controller. Both figures show that the new controller has improved disturbance rejection properties: The 7.4-mdeg maximum azimuth and elevation errors of the existing controller were reduced to 4.4-mdeg maximum azimuth and elevation errors in the new controller. Similarly, the 11-s settling time of the existing controller was reduced to 7 s with the new controller.

The responses of the antenna to the white-noise disturbances with the variance of 8.5 mdeg/s are shown in Figs. 20 and 21. The variances of the elevation error are 1.12 and 0.38 mdeg for the old and the new controllers, respectively. The variances of the azimuth error are 1.50 and 0.48 mdeg for the old and the new controllers, respectively. The figures and the variances show that the new controller noise-disturbance suppression improved threefold.

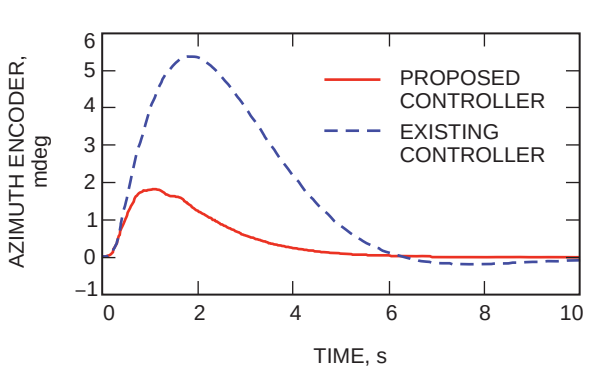

Fig. 18. The azimuth encoder response to the step disturbance of 0.01 deg/s for the proposed and existing controllers.

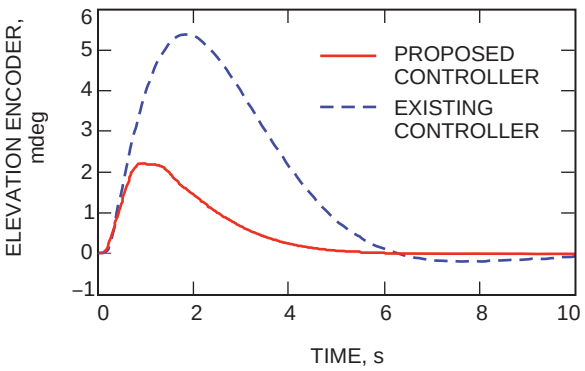

Fig. 19. The elevation encoder response to the step disturbance of 0.01 deg/s for the proposed and existing controllers.

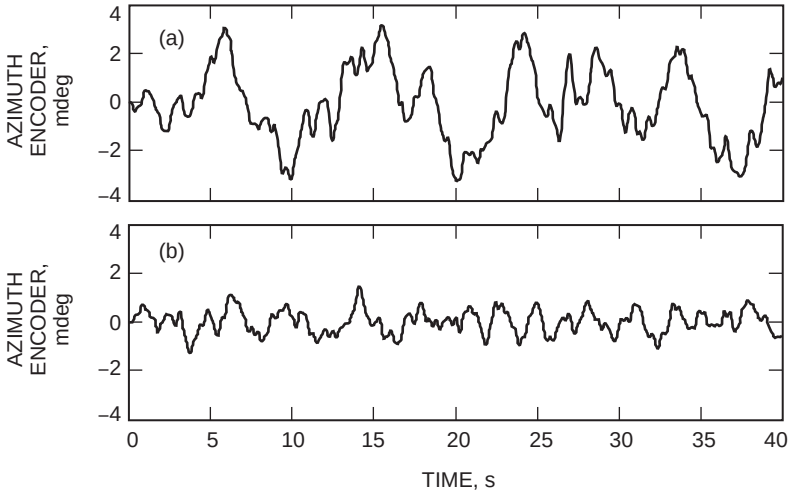

Fig. 20. The azimuth encoder response to the white-noise disturbance of 8.5-mdeg/s variance of the (a) existing and (b) proposed controllers.

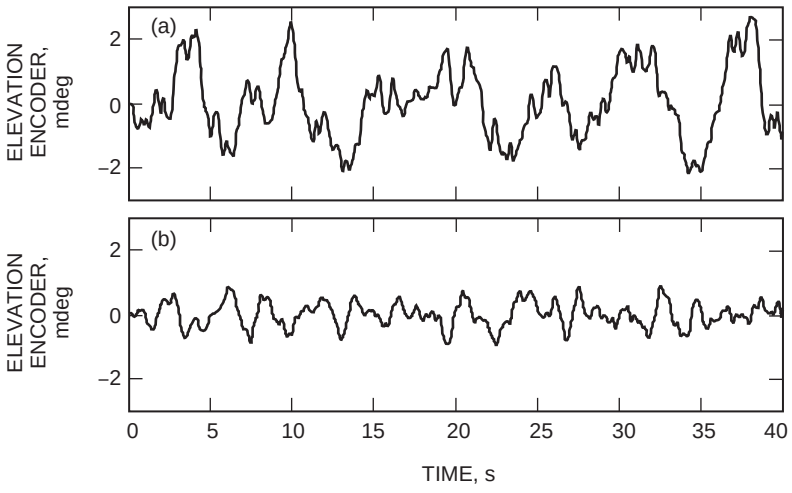

Fig. 21. The elevation encoder response to the white-noise disturbance of 8.5-mdeg/s variance of the (a) existing and (b) proposed controllers.

V. Conclusions

A new LQG controller for the DSS-14 antenna was designed and analyzed. It shows improved performance over the existing controller. However, due to its low acceleration limit, its implementation requires the development of the command preprocessor so that the slewing of the antenna will not exhibit limit cycling. The performance of the LQG controller can be enhanced further if necessary. This will require, besides analysis, field testing, since the high-performance controllers are more sensitive to the antenna-parameter variations. This controller was designed for the antenna "computer" (or encoder) mode. The development of the antenna "precision" mode controller will be similar, but it needs white-noise testing of the ME antenna mode. So far, this testing has failed, but a new approach that uses closed-loop white-noise testing has been successful at the DSS-23 antenna and can be used at DSS 14.

Acknowledgments

The authors would like to thank David Girdner and Robert Haroldsson for their help in the antenna testing.

References

[1] W. Gawronski and R. Bartos, "Modeling and Analysis of the DSS-14 Antenna Control System," *The Telecommunications and Data Acquisition Progress Report 42-124, October–December 1995*, Jet Propulsion Laboratory, Pasadena, California, pp. 113–142, February 15, 1996.

[2] J. N. Juang, *Applied System Identification*, Englewood Cliffs, New Jersey: Prentice Hall, 1994.

[3] W. Gawronski, *Balanced Control of Flexible Structures*, London: Springer Verlag, 1996.

[4] W. Gawronski and J. A. Mellstrom, "Control and Dynamics of the Deep Space Network Antennas," chapter in *Control and Dynamic Systems*, vol. 63, ed. C. T. Leondes, San Diego: Academic Press, 1994.

[5] W. Gawronski, "Wind Gust Models Derived From Field Data," *The Telecommunications and Data Acquisition Progress Report 42-123, July–September 1995*, Jet Propulsion Laboratory, Pasadena, California, pp. 30–36, November 15, 1995.